MENGZE HAN, who is an intermediate engineer with a Master's degree, is currently a lecturer in the School of Civil Engineering at the Shangqiu Institute of Technology where he received the Institute's Excellent Teacher Award for two consecutive years. He has many years of teaching and engineering practice experience, with his main research focus being on civil engineering, surveying and mapping. He is the director of the Civil Engineering Architectural Society of Shangqiu, and also serves on the editorial board of the magazine *Kohai Story Expo*.

Contact details:
School of Civil Engineering
Shangqiu Institute of Technology
No 236 Middle Section of Suiyang Avenue
Shangqiu City, Henan Province, Shangqiu, China 476000
E-mail: m15137035991_1@163.com

ZICONG MA is an undergraduate student at Guilin University of Technology, mainly focusing on the mechanical properties of civil engineering structures.

Contact details:
School of Civil and Architectural Engineering
Guilin University of Technology
No 12 Jiangan Road, Qixing District, Guilin City
Guangxi Zhuang Autonomous Region, Guilin, China 541004
E-mail: mzctvaa@163.com

QIRONG QIU is an engineer from Shanghai Construction Engineering Group, and acted as the corresponding author of this paper. He is mainly engaged in construction and design in the housing sector, but also focuses on researching civil engineering structures.

Contact details:
Shanghai Construction Engineering Fifth Construction Group Co Ltd
Shanghai Construction Engineering Co Ltd
Shanghai Institute of Technology, Shanghai, China 200063
E-mail: m15296852294@163.com / 712074154@qq.com

PENGCHENG LIAO is an engineer at the Third Construction Engineering Co Ltd of the Guangxi Construction Engineering Group. He graduated from Guilin University of Technology, and is mainly engaged in the construction and design of industrial and migrant buildings, with a research focus on the design and development of civil engineering structures.

Contact details:
Guangxi Construction Engineering Group
Third Construction Engineering Co Ltd
16 Guiya Road, Qingxiu District, Nanning City
Guangxi Zhuang Autonomous Region, Nanning, China 545000
E-mail: 17687438787@163.com

Research on seismic performance and axial compression ratio of rectangular high-strength spiral stirrup confined concrete columns

M Han, Z Ma, Q Qiu, P Liao

Replacing traditional stirrups with high-strength rectangular spiral stirrups can improve the seismic performance of reinforced concrete columns. In order to study the seismic performance of high-strength spiral stirrup confined concrete columns, a validated finite element (FE) method was proposed to establish the FE model of reinforced concrete columns. Combined with the measured data of two existing specimens, parameter analysis was conducted on 19 specimens. The axial compression ratio, shear span ratio, stirrup spacing, and stirrup diameter were variable parameters. Based on a reliable model, internal stress analysis was conducted, and the influence of different variables on the seismic performance of reinforced concrete columns was revealed. The FE results suggest that, when the axial compression ratio is not greater than 0.6, the requirement of ductility greater than 3 in the Chinese Standard GB 50011-2010 can be met. The recommended shear span ratio for optimal ductility was around 4.5. The reinforcement ratio of high-strength spiral stirrups ranges from 1.0% to 2.2%. After completing the simulation of nearly 100 specimens (only calculating the ductility coefficient), a matching relationship between the axial compression ratio limit and the shear span ratio was proposed.

Keywords: rectangular spiral stirrup, high-strength reinforcement, seismic engineering, numerical method, ductility

INTRODUCTION

Early in the 20th century the concept of confined concrete was proposed, which utilises external lateral confinement to improve the brittleness of concrete itself, and enhance its strength and increased ductility (Mander *et al* 1988). It has become an important measure to improve the mechanical properties of components in engineering (Cao *et al* 2019; Jing *et al* 2020). As is well known, concrete can significantly enhance its strength and ductility under effective lateral confinement.

The use of spiral stirrups to provide lateral restraint for core concrete was one of the common ways to improve the strength and deformation performance of concrete (Mander *et al* 1988). Zongping Chen *et al* (Chen 2021a; 2021b; 2022a;

2022b; 2022c; 2022d) conducted extensive experiments, numerical simulations, and theoretical studies on reinforced concrete columns with built-in circular spiral hoops. The presence of spiral hoops improved the confinement on the concrete core, significantly improving the bearing capacity and deformation resistance of concrete columns. In addition to circular spiral stirrups, rectangular spiral stirrups are also a form of spiral reinforcement. Rectangular spiral stirrups have the advantages of simple binding and good cross-sectional adaptability, and can be applied to various regular structures. The built-in spiral stirrups not only provide effective confinement for concrete, but also facilitate construction, eliminating hooks at corners, and optimising steel usage. Guo *et al* (2001)

first conducted low-cycle repeated tests on frames with rectangular spiral stirrups, and the results showed that square spiral stirrups, especially composite square spiral stirrups, can effectively avoid the loosening and straightening phenomenon of ordinary stirrups, prevent lantern-shaped damage, and effectively improve the hysteresis performance of frame columns after peak load. On this basis, the axial compression and seismic resistance of concrete columns confined by rectangular spiral stirrups were studied, and the research by Xue *et al* (2016; 2019; 2020) and Chen *et al* (2015) demonstrated that, compared with ordinary stirrups, spiral stirrups provide stronger lateral confinement, and thus the reinforced concrete column has better deformation performance. Furthermore, they also proved that the ultimate bearing capacity of specimens with rectangular spiral stirrups increases as the concrete strength and volumetric stirrup ratio increase.

However, in order to meet the demands of practical engineering, the columns of bridges and super-high-rise buildings need to bear significant loads. As a result, the cross-section of these structures will be larger, which may compromise aesthetics and pose challenges in actual construction. It is necessary to replace ordinary strength steel bars with high-strength steel bars (Aboukifa & Moustafa 2021; Yang *et al*

2022). Su *et al* (2014) used high-strength stirrups in concrete and found that the use of high-strength stirrups can reduce the amount of steel bars used. Zhang *et al* (2013) conducted seismic tests on four high-strength spiral reinforced concrete columns to investigate the impact of axial compression ratio and stirrup strength. The experimental findings suggest that high-strength stirrups enhance the ductility and energy dissipation capacity of concrete columns, even when subjected to the same axial compression ratio. This is due to the increase in steel bar strength and the constraint of rectangular spiral stirrups. In addition, Zhao *et al* (2019) conducted seismic performance tests on reinforced concrete walls equipped with high-strength rectangular spiral stirrups. Compared to traditional steel, high-strength steel typically exhibits lower ductility. However, the above studies have shown that the ductility of reinforced concrete columns can still meet Chinese standard GB 50011-2010 (Chinese Standard 2010b) by using high-strength rectangular spiral stirrups.

While rectangular high-strength spiral stirrups show promise in their application, there has been limited research conducted on them. Therefore, it is crucial to investigate the influence of various factors such as axial compression ratios, shear span ratios, spacing of rectangular spiral stirrups, and the diameter of rectangular spiral stirrups

on the seismic performance of reinforced concrete columns. In order to further study the seismic performance of rectangular high-strength spiral reinforced concrete columns, finite element (FE) analysis methods were adopted. Firstly, the experiment conducted by Zhang *et al* (2013) was modelled and validated using their experimental results. On the basis of a reliable model, 19 specimens (including 2 test specimens and 17 numerical simulation analysis specimens) were thoroughly analysed. The axial compression ratio, shear span ratio, stirrup spacing, and stirrup diameter were studied as key factors, and the effects of different variables on the seismic behaviour of rectangular high-strength spiral reinforced concrete columns were revealed. A large number of verification calculations have been carried out, and the matching relationship between the axial compression ratio limit and the shear span ratio has been proposed, aiming to provide reference for engineering.

INTRODUCTION TO PREVIOUS EXPERIMENTS

Two rectangular high-strength spiral stirrup reinforced concrete columns with axial compression ratios of 0.18 and 0.55 were designed by Zhang *et al* (2013), and the cross-sectional design is shown in Figure 1. The calculation method for axial compression ratio *n* and shear span ratio λ is shown in Equations 1 and 2, respectively. Table 1 provides detailed design parameters for the specimens and FE simulation specimens. The cross-sectional dimensions of all specimens were designed to be 400 mm × 400 mm; the height from the centre of the electro-hydraulic servo actuator to the surface of the ground beam was designed to be 1 800 mm. Eight HRB400 grade steel reinforcement with a diameter of 22 mm were used as longitudinal steel bars, and high-strength steel bars with a diameter of 5 mm were used as internal rectangular spiral stirrups. The reinforcement ratio and hoop ratio are designed according to the GB 50010-2010 (Chinese Standard 2010a), meeting the minimum requirements. The basic mechanical properties of the test material are shown in Table 2.

$$n = \frac{N}{A_c \cdot f_c} \qquad (1)$$
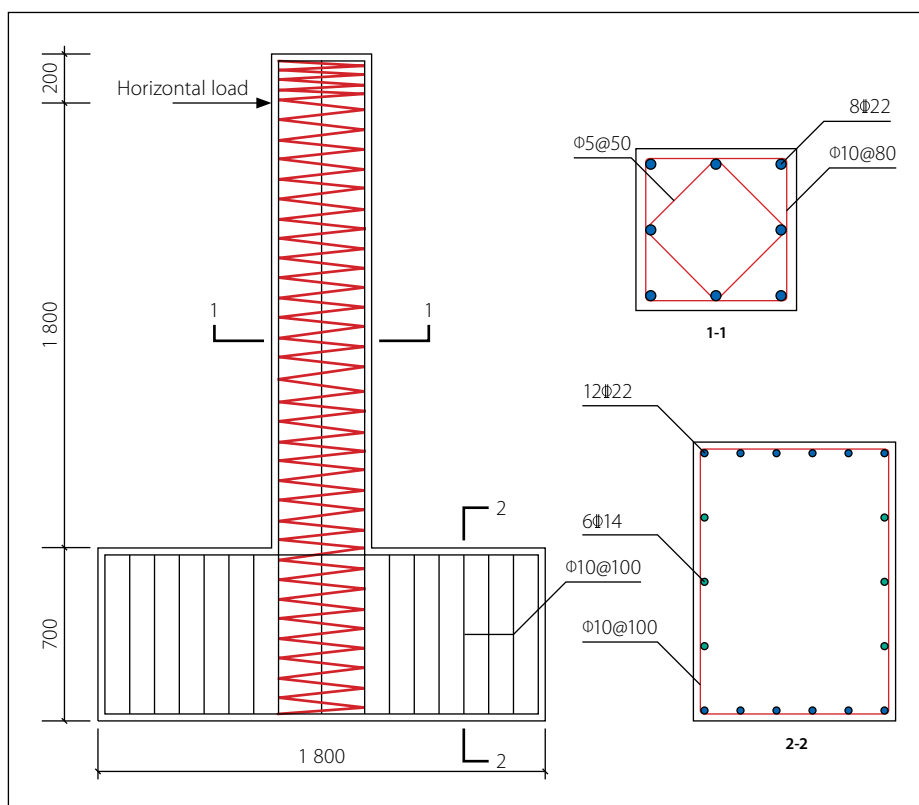
$$\lambda = \frac{L}{a} \qquad (2)$$

Figure 1 Structural diagram of specimen (adapted from Zhang *et al* 2013)

Table 1 Parameters and results of the specimen

Specimen no	Axial compression ratio n	Calculated length L/mm	Shear span ratio λ	Spiral stirrup spacing S/mm	Spiral stirrup diameter d_{st}/mm	P_p/kN	μ	Notes
HSSC-01	0.18	1 800	4.5	50	5	218.89	5.43	Reference (Zhang *et al* 2013)
HSSC-02	0.55	1 800	4.5	50	5	284.80	2.90	
FE-1	0.18	1 800	4.5	50	5	215.2	5.60	Change in axial pressure ratio
FE-2	0.4	1 800	4.5	50	5	211.3	4.01	
FE-3	0.6	1 800	4.5	50	5	203.3	2.73	
FE-4	0.8	1 800	4.5	50	5	195.0	2.53	
FE-5	0.9	1 800	4.5	50	5	190.9	2.47	
FE-6	0.18	1 000	2.5	50	5	412.0	4.51	Change in shear span ratio
FE-7	0.18	1 400	3.5	50	5	283.4	5.41	
FE-8	0.18	2 600	6.5	50	5	134.3	5.28	
FE-9	0.18	3 400	8.5	50	5	96.4	3.48	
FE-10	0.18	1 800	4.5	30	5	216.5	5.95	Change in spacing of spiral stirrups
FE-11	0.18	1 800	4.5	70	5	211.6	5.05	
FE-12	0.18	1 800	4.5	100	5	210.6	4.60	
FE-13	0.18	1 800	4.5	150	5	209.7	4.38	
FE-14	0.18	1 800	4.5	50	8	225.6	6.86	Change in diameter of spiral stirrups
FE-15	0.18	1 800	4.5	50	10	231.7	6.88	
FE-16	0.18	1 800	4.5	50	12	241.6	6.91	
FE-17	0.18	1 800	4.5	50	14	243.6	6.97	

Where:

N is the applied axial pressure

n is the axial compression ratio

A_c and f_c are the cross-sectional area and axial compressive strength of the concrete, respectively

$λ$ is the shear span ratio

L is the height from the loading point to the surface of the base

a is the side length of the section.

The base of the specimen was fixed to the ground through high-strength screws to minimise horizontal displacement of the base. The vertical load was applied by a hydraulic jack at the top of the column to the designed axial compression ratio, and it remained stable throughout the entire test process. After the vertical load had been applied, the horizontal load was then applied by the electro-hydraulic servo actuator. The horizontal load adopts a joint control loading scheme of force and displacement. A horizontal load in increments of 50 kN is applied using load control until the specimen begins to yield. After the specimen yields, displacement control loading is applied, with each loading increment being a multiple of the yield displacement. For instance, if the yield level displacement of the specimen is denoted as Δ_y, the loading is conducted

Table 2 Properties of materials

Material type	Yield strength f_y/MPa	Ultimate strength f_u/MPa	Elastic modulus E_0/GPa	Cube compressive strength f_{cu}/MPa	Cylinder compressive strength f_c/MPa
HRB400	490	663	201	-	-
high-strength stirrup	1 052	1 173	206	-	-
concrete	-	-	31.1	43.8	29.3
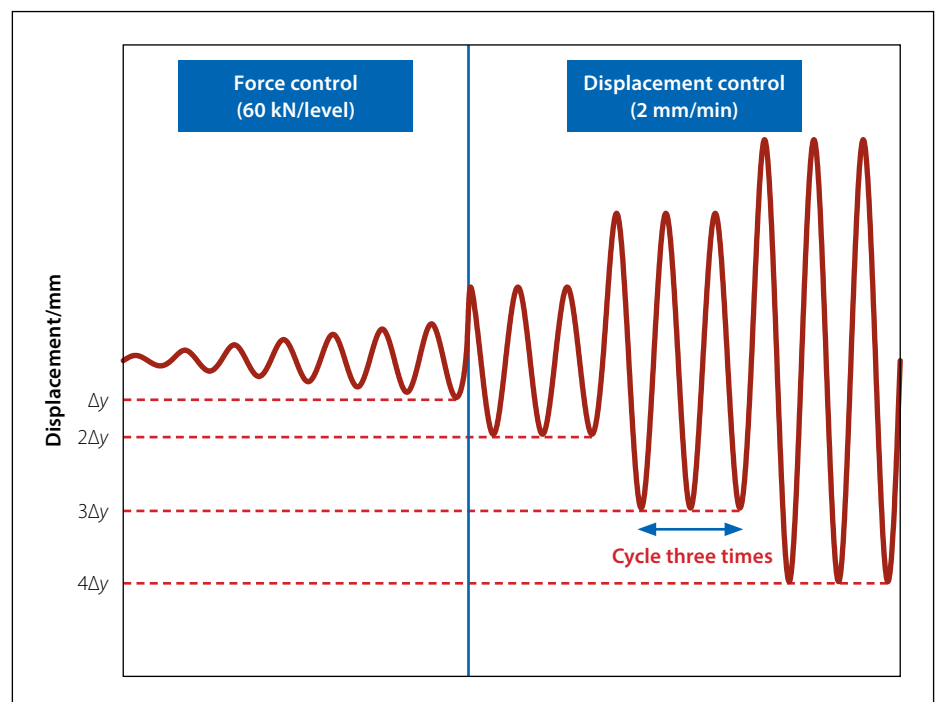
Figure 2 Loading system

Table 3 Element type selection

Materials	Concrete	Reinforcement
Strength grade	C40	HRB400 / High-strength steel
Selected element	C3D8R	T3D2

at $2\Delta_y$, $3\Delta_y$, $4\Delta_y$, and so on. The loading rate is 2 mm/min. The loading and unloading of each stage were repeated three times. The loading system is shown in Figure 2.

FINITE ELEMENT ANALYSIS

General

The FE software of Abaqus/Standard was employed to build the FE models. The concrete and steel reinforcement were combined into an FE model. The size of each component is consistent with the experiment. Figure 3 presents a comparison of calculation results obtained using different mesh sizes. It is evident from the figure that the calculation results exhibit a high level of consistency when the model is divided into mesh with a size of 50 mm. Longitudinal bars, stirrups, and rectangular spiral stirrups were embedded in concrete, and the bond slip between them was ignored. Table 3 shows the element types selected for each part.

Materials

Steel

The bilinear model of strain hardening was adopted as the constitutive model of steel in ABAQUS/CAE, without considering large deformation of the material. Equation 3 provides the calculation formula for the constitutive relationship of steel. The schematic diagram of the constitutive relationship is shown in Figure 4 (Chen *et al* 2021; 2022). The required values for ABAQUS were obtained through experimental measurements, and the values are shown in Table 2.

$$\sigma = \begin{cases} E_0\varepsilon & (0 \le \varepsilon \le \varepsilon_y) \\ f_y + E_s(\varepsilon - \varepsilon_y) & (\varepsilon_y \le \varepsilon) \end{cases} \quad (3)$$

Concrete

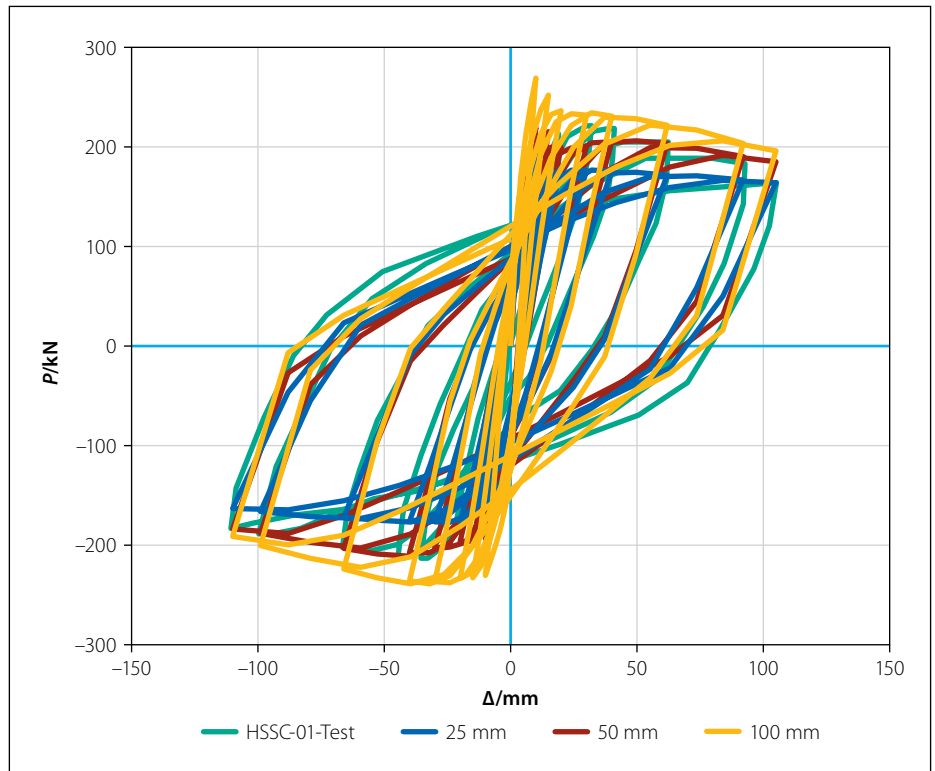In this paper, the concrete plastic damage model (CDP) in ABAQUS 2020 was

Figure 3 Comparison of calculation results with different mesh sizes

adopted. The stress-strain relationship of concrete proposed in the GB50010-2010 Code for Design of Reinforced Concrete Structures (GB50010-2010) was adopted, as shown in Equations 4 and 5 where f_c and ε_c are the ultimate compressive stress and strain of concrete, and α_a and α_d are parameters for the rising and falling segments, respectively. According to GB50010-2010, when using C40 grade concrete, they are taken as 2.03 and 1.36 (Chinese Standard 2010a).
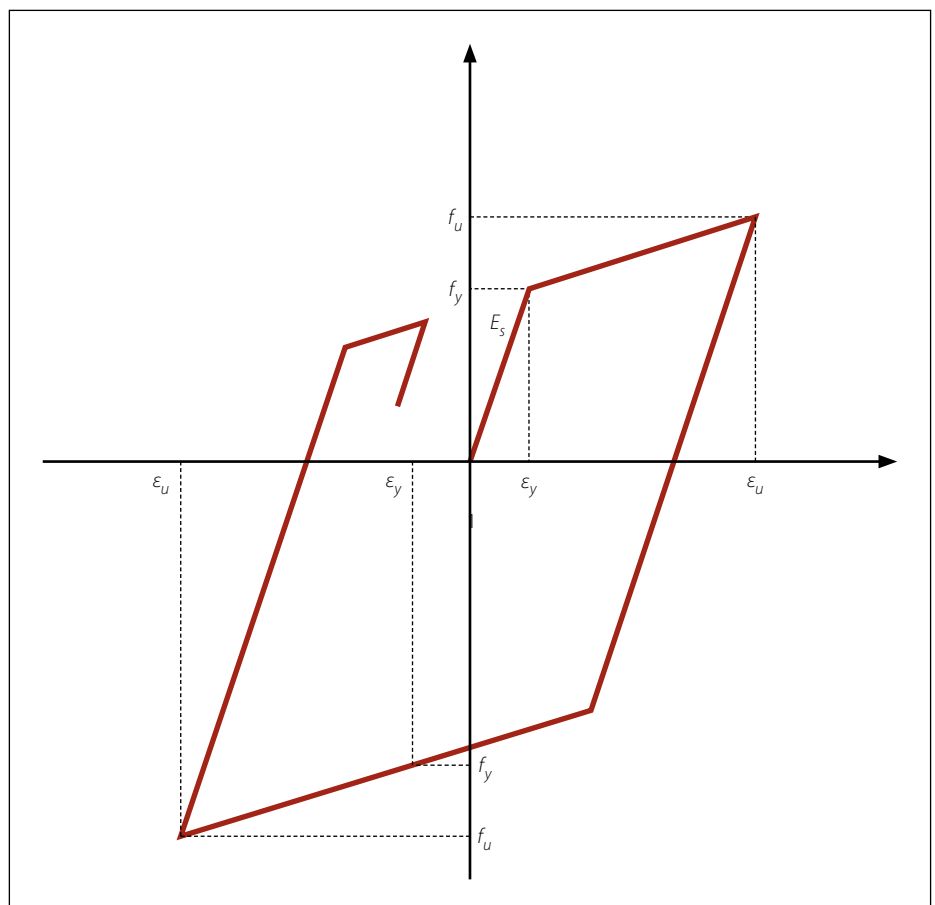

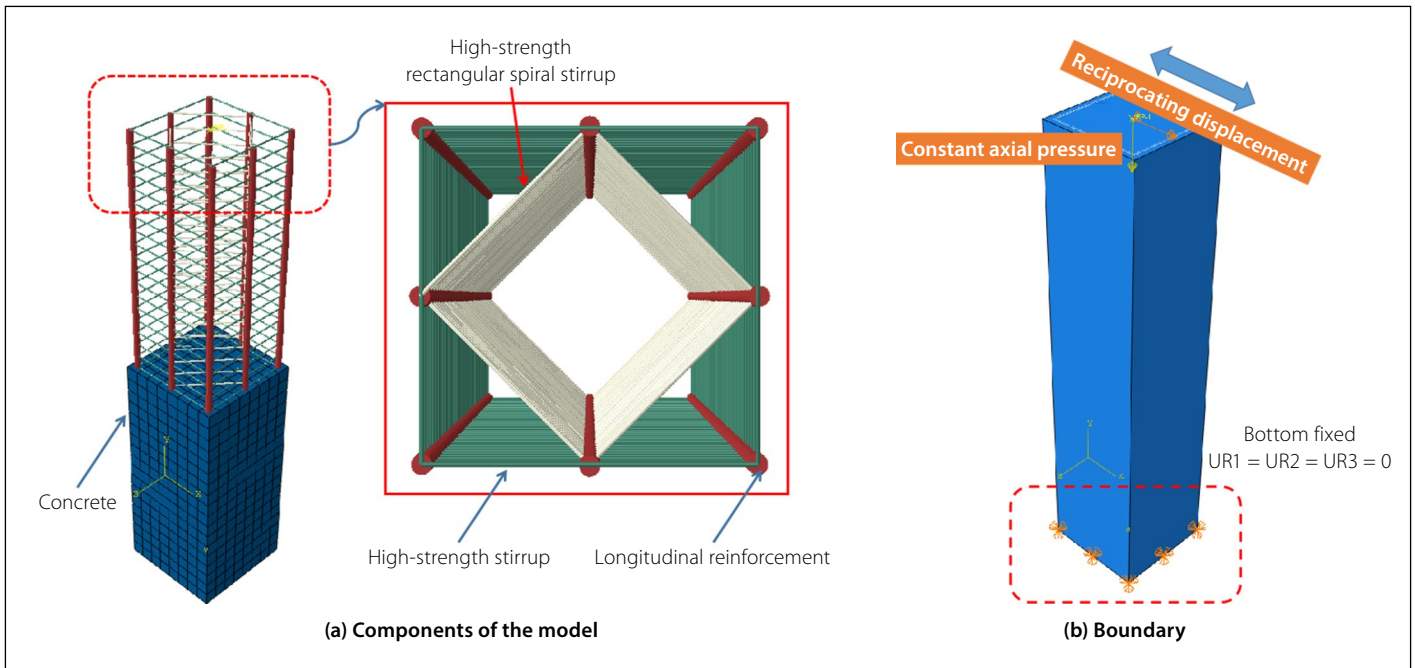**Figure 4** Elastic-plastic model (adapted from Chen *et al* 2021; 2022)

(a) Components of the model

(b) Boundary

Figure 5 Mesh generation and boundary conditions of FE model

$$y = \begin{cases} a_a x + (3 - 2a_a)x^2 + (a_a - 2)x^3 \\ \qquad\qquad\qquad\qquad 0 \le x \le 1\varepsilon \\ \dfrac{x}{a_d(x - 1)^2 + x} \qquad x \ge 1 \end{cases} \quad (4)$$

$$y = \frac{\acute{o}}{f_c}, \quad x = \frac{\varepsilon}{\varepsilon_e} \qquad (5)$$

Numerical model

In the construction of the numerical model of the seismic test, the loading beams and ground beams can be omitted. The top of the test column was equipped with a coupling reference point that can simultaneously constrain the torsion angle and horizontal displacement. Therefore, the length of the model was calculated as 1 800 mm, as was shown in Figure 1. Horizontal displacement and constant axial pressure were applied to the top of the column, while the boundary condition at the bottom of the column was fixed against translation and rotation. The constant axial pressure at the top of the column is 843 kN when the axial compression ratio is 0.18, and 2 578.4 kN when the axial compression ratio is 0.55. The model establishment was completed as shown in Figure 5.

Model validation

The experimental results obtained from Zhang *et al* (2013) were used to validate the numerical models used in this research. Figures 6 and 7 provide a comparison of the hysteresis and skeleton curves between the experiment and simulation. The hysteresis curve calculated using the FE method is consistent with the experimental results, showing a similar pinching effect, that is, the hysteresis curve is shuttle-shaped. The simulated hysteresis curve's wrapping area, loading stiffness, and unloading stiffness are basically consistent with the experimental results. The simulated skeleton curve trend was highly consistent with the ultimate shear bearing capacity. The reason for a certain deviation between the bearing capacity and initial stiffness and the test results may be that the bond slip was not
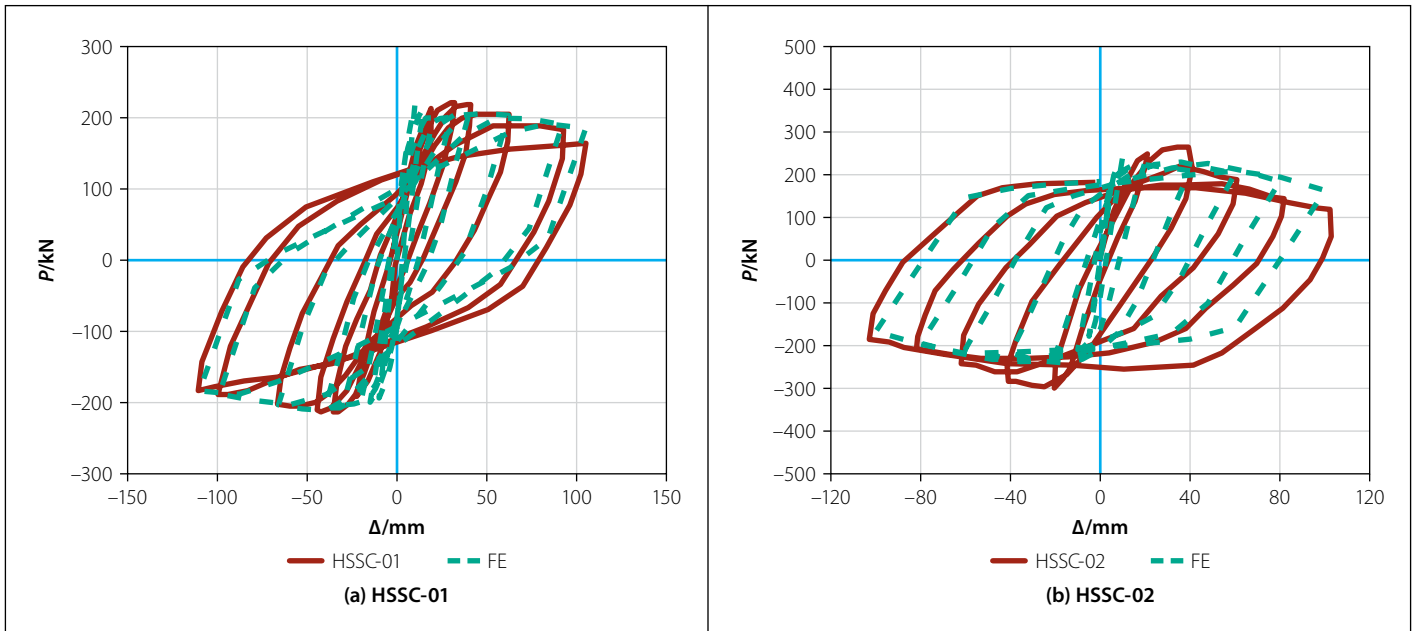

(a) HSSC-01

(b) HSSC-02

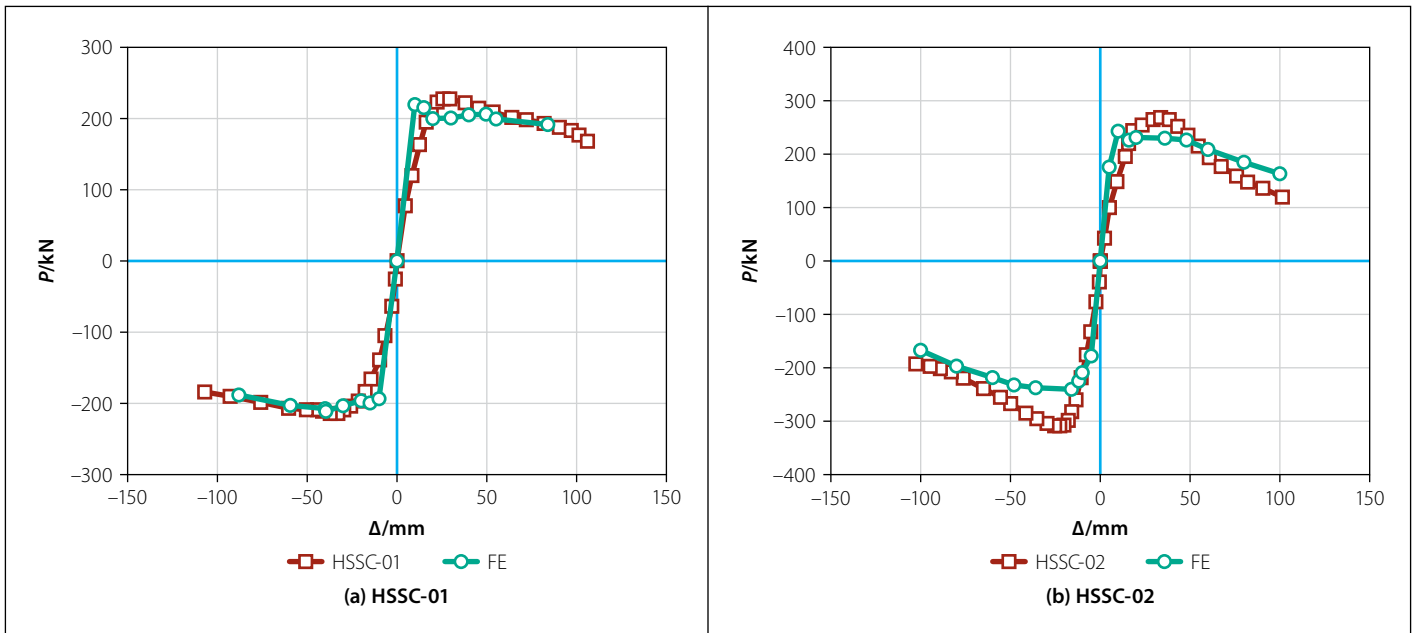**Figure 6** Comparison of experimental and simulated hysteresis curves

Figure 7 Comparison of experimental and simulated skeleton curves

considered. On the other hand, the simulated boundary conditions assume that the bottom of the column is completely rigid, and there will inevitably be slight deformation during the experimental process. The model conditions perfectly ignored the gaps between the loading devices, resulting in a higher loading stiffness.

Figure 8 compares the tensile damage of concrete calculated by the model with the development of concrete cracks in the experiment. It can be seen from the figure that the tensile damage contour of concrete obtained from the FE results was very similar to the crack diagram of the test results. There were interval cracks in the concrete, and it was observed that the distance between the cracks was close to the distance between the spacing of spiral stirrups. On the other hand, concrete collapse at the column base under high axial compression ratio was also observed, similar to the concrete peeling in the experiment. Due to the inability of ABAQUS software to consider concrete cracking, concrete cracking can only be considered by defining the tensile damage of concrete. Therefore, it can be seen in the hysteresis curve and skeleton curve that the simulated stiffness will be slightly greater than the experimental value. The measured ultimate bearing capacity and ductility of HSSC-01 and HSSC-02 are shown in Table 1. The ultimate shear bearing capacity of HSSC-01 and HSSC-02 measured in the FE analysis was 215.2kN and 257.8kN, respectively, and the ductility coefficients were 5.60 and 2.85, respectively. The average error was within 10%, indicating that the model can
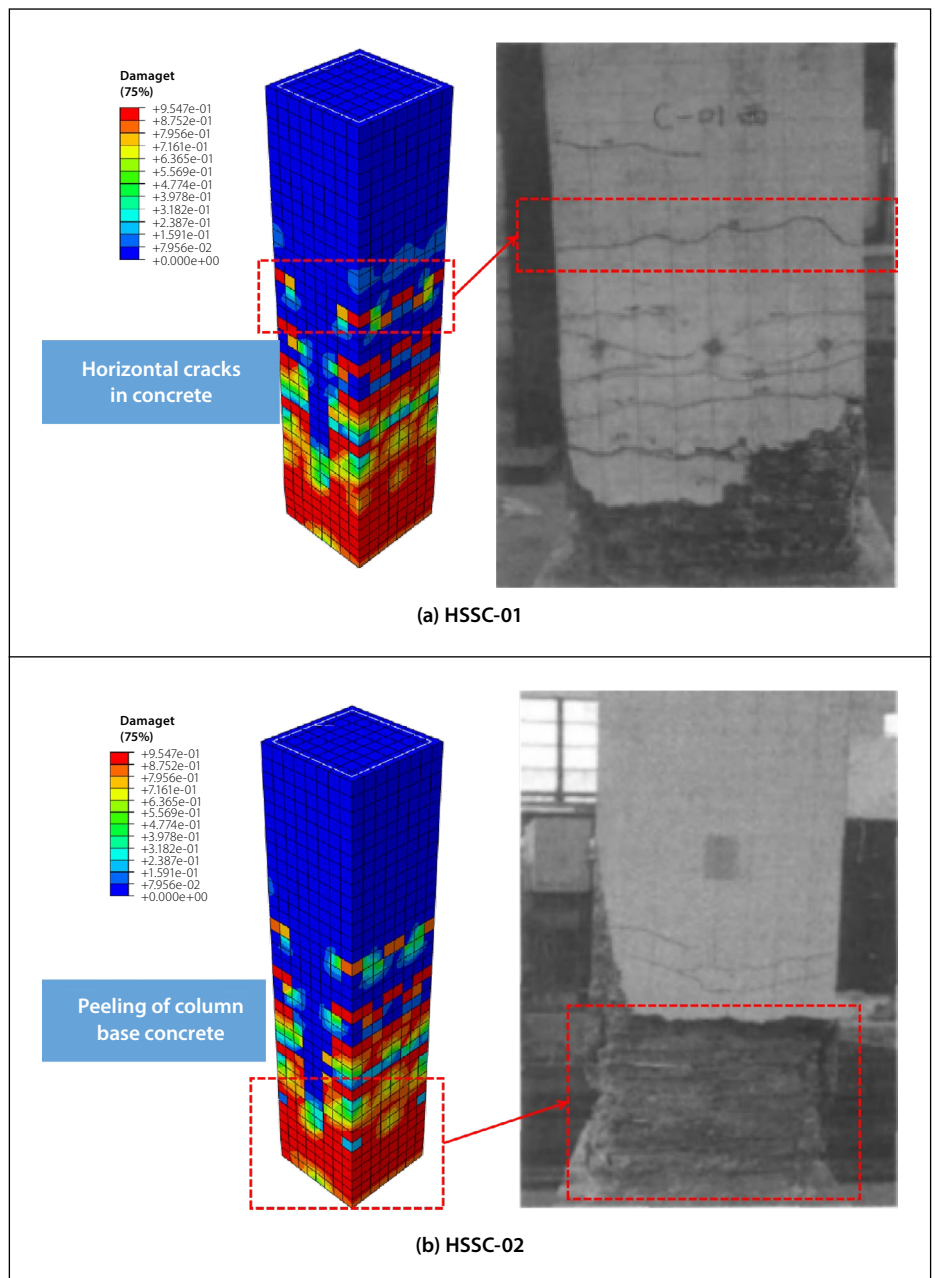

Figure 8 Comparison of failure modes (adapted from Zhang *et al* 2013 with permission)
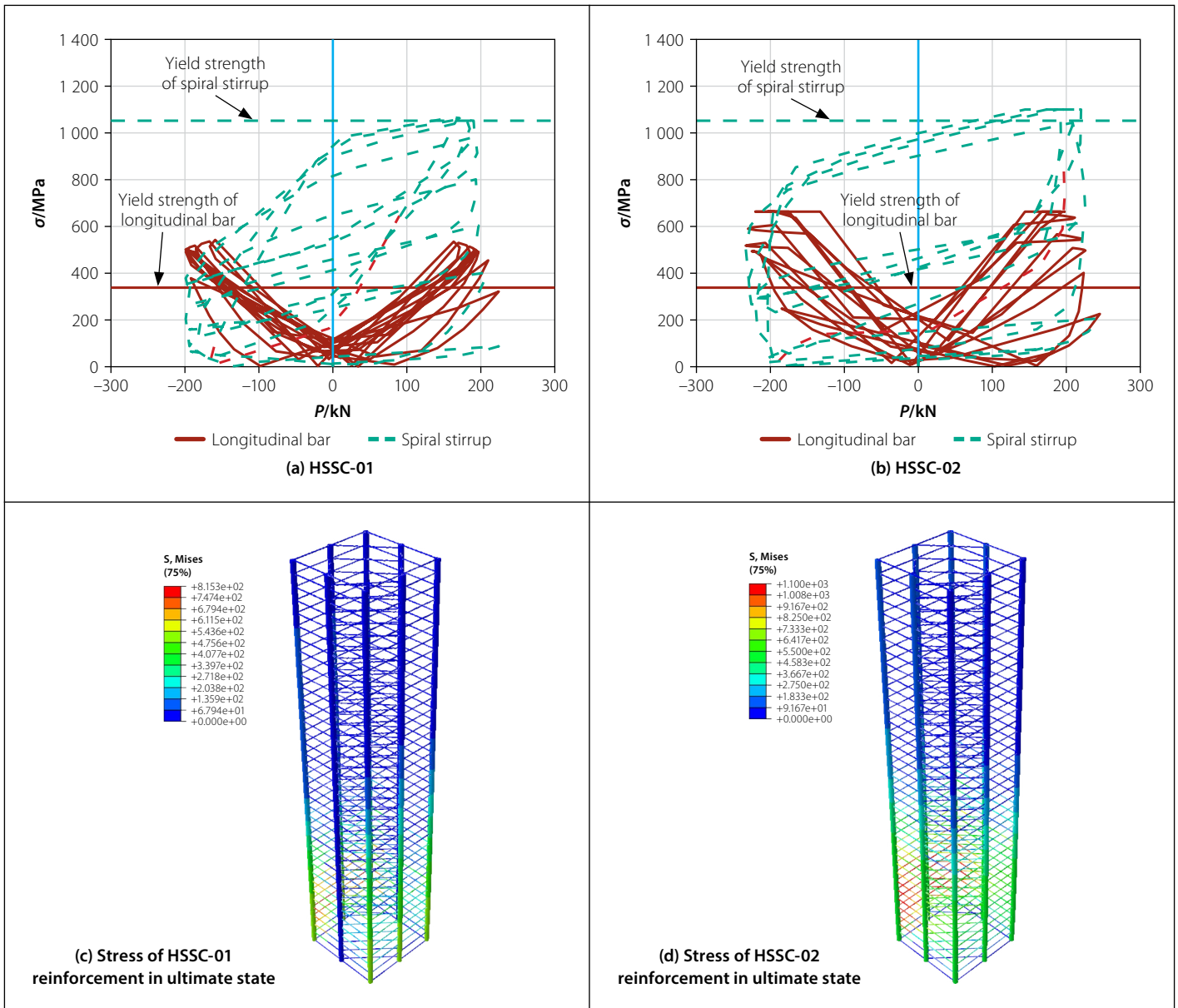
Figure 9 Stress variation curve and stress cloud diagram

Stress analysis

Figures 9(a) and 9(b) show the stress curves of the longitudinal steel bars and high-strength spiral stirrups extracted from the FE model. The data points taken were the stress of the steel reinforcements under forward loading and compression. The longitudinal reinforcement stress curve was symmetric about the coordinate axis, while the stress-strain curve of rectangular high-strength spiral stirrups yields on the compressive side. This indicates that during the entire stress process, the high-strength rectangular spiral stirrups mainly increase the confinement on the compression side, and the tensile stress on the tension side is provided by the longitudinal bars. Within the experimental range, the yield rate of longitudinal steel bars and spiral

stirrups increases with the increase of axial compression load. This is because of the existence of the Poisson effect. When the column is compressed, it tends to expand transversely in tension, which is resisted by the confinement provided by the stirrups. Conversely, when the column is in tension, the transverse direction experiences compression (column width gets narrower), and the core of the column provides sufficient restraint and therefore the stress in the stirrups is lower.

Figures 9(c) and 9(d) show the stress cloud diagrams of steel bars at peak load for specimens. As shown in the figure, when the peak load was reached, the rectangular spiral stirrups of the small axial compression ratio specimens did not yield, while the high axial compression ratio specimens yielded due to the confinement provided by the stirrups, indicating that the high-strength spiral stirrups can fully exert

their material properties under high axial compression ratios.

PARAMETER ANALYSIS

The model HSSC-01 specimen was selected as the reference model, and 17 models were designed and calculated with the axial compression ratio n, shear span ratio λ, stirrup spacing S, and stirrup diameter d_{st} as the variable parameters. Specific parameters and characteristic points of calculation results are shown in Table 1.

Hysteresis curve and skeleton curve

Figures 10 and 11 show the comparison of hysteresis curves and skeleton curves for each specimen. By comparing different variation parameters, the following conclusions can be drawn:

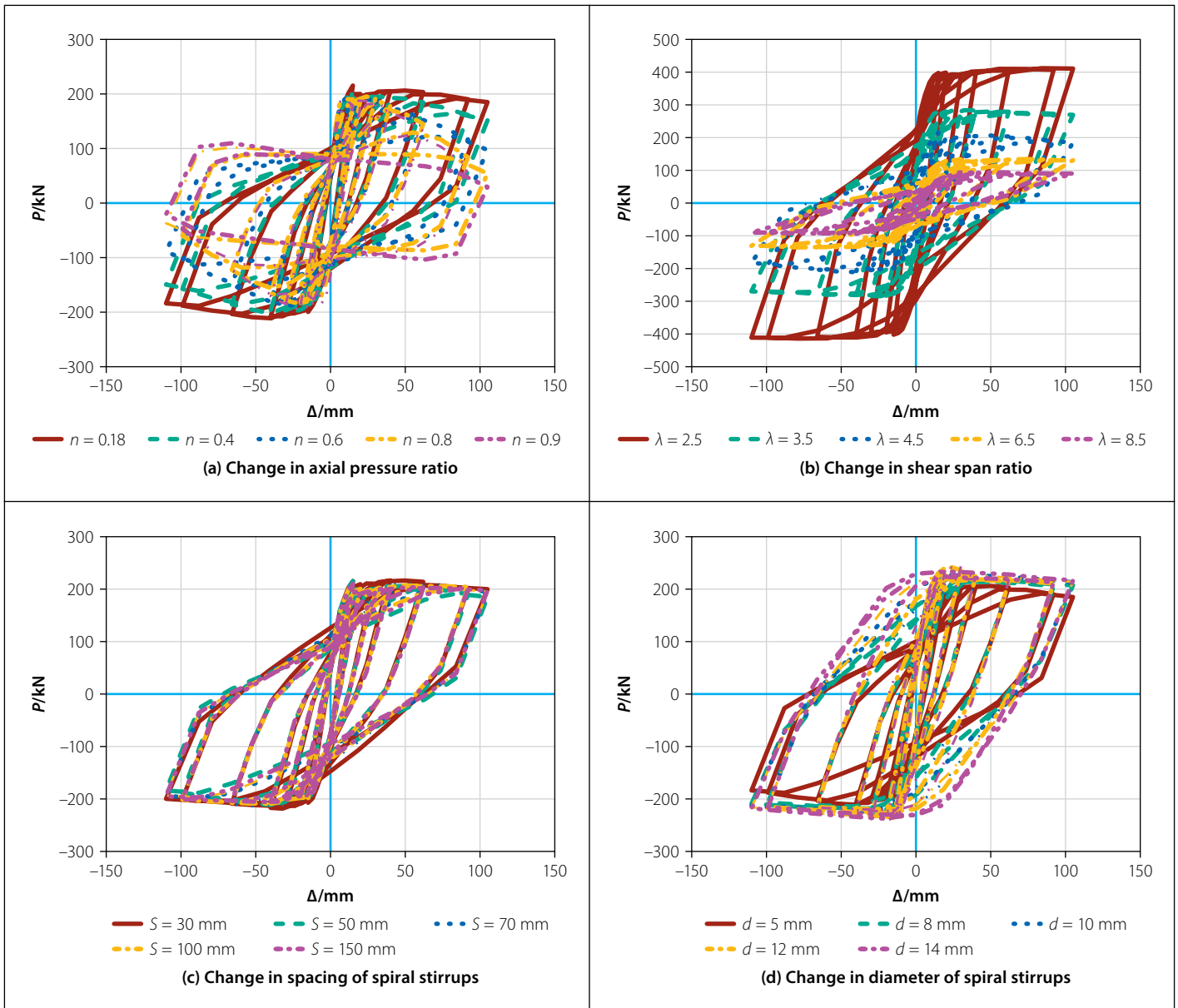1. The ultimate bearing capacity and hysteresis curve shape of the specimen

Figure 10 Hysteresis curve

are not significantly affected by the axial compression ratio, but an increase in the axial compression ratio leads to a greater slope in the descending section of the curve, resulting in significant degradation of ductility.

2. As the spacing of spiral stirrups increases, the envelope area of the hysteresis curve decreases, resulting in a decrease in the ultimate bearing capacity. This is due to the reduced constraint on the core concrete caused by the increased spacing of spiral stirrups. Consequently, the energy dissipation capacity and bearing capacity are negatively affected. The shape of the hysteresis curve of the specimen becomes fuller with the increase of the diameter of the rectangular high-strength spiral stirrup, indicating better energy dissipation capacity. Increasing the diameter of rectangular spiral stirrups is more effective

in improving seismic performance than reducing the spacing diameter of rectangular spiral stirrups.

Shear capacity and ductility

The average values of positive and negative bearing capacity and ductility coefficient of all specimens are shown in Table 1. The effects of different variables were compared, and the following conclusions were obtained:

1. The ultimate bearing capacity of the specimens with $n = 0.4$, 0.6, 0.8 and 0.9 decreased by 1.9%, 5.6%, 9.4% and 11.3%, and the ductility decreased by 28.4%, 51.3%, 54.8% and 55.9%, respectively, compared to the specimens with $n = 0.18$. The axial compression ratio is a key influencing factor on the seismic performance of rectangular high-strength spiral reinforced concrete columns. According to the requirement

of ductility coefficient greater than 3 in the specification GB 50011-2010 (Chinese Standard 2010b), the limit value of the experimental axial compression ratio is $n = 0.4 \sim 0.6$.

2. The ultimate bearing capacity degradation of reinforced concrete columns with $\lambda = 3.5$, 4.5, 6.5 and 8.5 reached 31.3%, 47.8%, 67.5% and 76.7%, compared to specimens with $\lambda = 2.5$. The ductility shear span ratio increases first and then decreases, reaching its maximum value at $\lambda = 4.5$, indicating that the shear span ratio is optimal for rectangular high-strength spiral reinforced concrete columns.

3. Compared with specimens with $S = 30$ mm between stirrups, the ultimate bearing capacity of specimens with $S = 50$ mm, 70 mm, 100 mm and 150 mm decreased by 0.7%, 2.3%, 2.8% and 3.2%, respectively, and the ductility
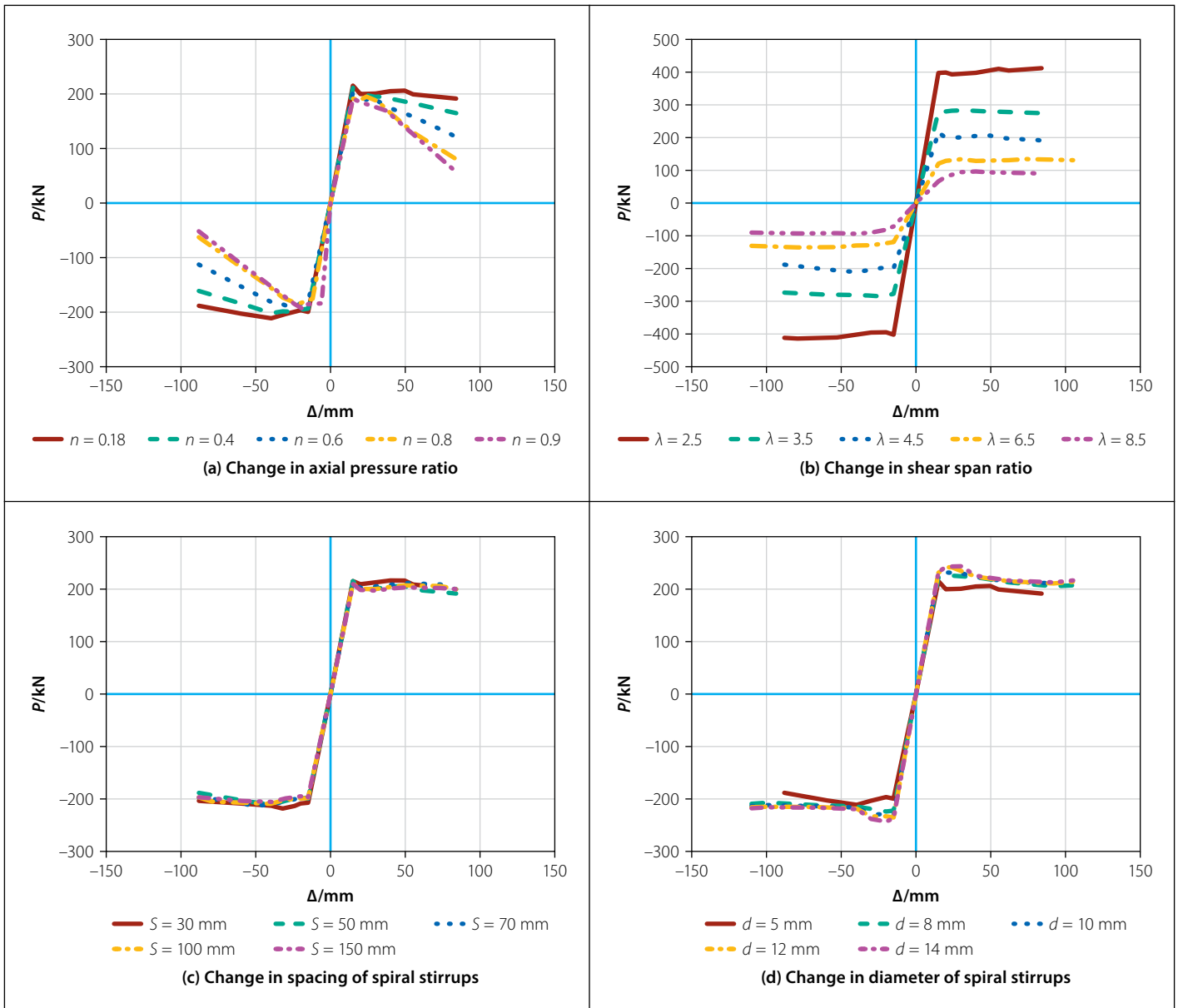
Figure 11 Skeleton curve

decreased by 5.9%, 15.2%, 22.7% and 26.4%. Overall, the change in stirrup spacing has little effect on the bearing capacity, mainly because when the shear span ratio is 4.5, the specimen undergoes bending failure, and its bearing capacity is mainly provided by the longitudinal reinforcement. The reason for the significant decrease in ductility may be that spiral stirrups have a strong confining effect on concrete, and the reduction in stirrup spacing enhances the crack resistance of concrete, thereby improving the ductility of the specimen. The reduction in the stirrup spacing also increases the effective core area that is confined due to the arching action between the stirrups

4. As the diameter of the rectangular high-strength spiral stirrup increases, the ultimate bearing capacity and ductility of the specimen gradually increase.

Compared with the specimen with d_{st} = 5 mm, the ultimate bearing capacity of the specimen with d_{st} = 8 mm, 10 mm, 12 mm and 14 mm increases by 4.8%, 7.6%, 12.2% and 13.1%, respectively, and the ductility increases by 22.5%, 22.8%, 23.3% and 24.4%, respectively. Overall, when the diameter of the rectangular high-strength spiral stirrup increases from 12 mm to 14 mm, the efficiency of increasing the bearing capacity of the specimen is the lowest, only 0.9%, and the increase in ductility is between 22.5% and 24.4%. Therefore, it is recommended that the diameter of the stirrup be between 8 mm and 12 mm (at this time the volumetric reinforcement ratio is between 1.0% and 2.2%).

Stiffness degradation

The stiffness degradation curves of all specimens are shown in Figure 12. The

calculation method is to take the secant stiffness at the peak point of each level of the skeleton curve as the shear stiffness of that level:

$$K = \frac{|+P_i| + |-P_i|}{|+\Delta_i| + |-\Delta_i|} \qquad (6)$$

Where: Δ_i and P_i are the maximum displacement and load corresponding to the level i cycle, respectively, and + and – indicate forward and reverse loading, respectively.

The following conclusions can be drawn by comparing different variation parameters:

1. The larger the n, the greater the initial stiffness, but the faster the degradation rate. When the horizontal displacement is greater than 50 mm, the secant stiffness decreases as the n increases.

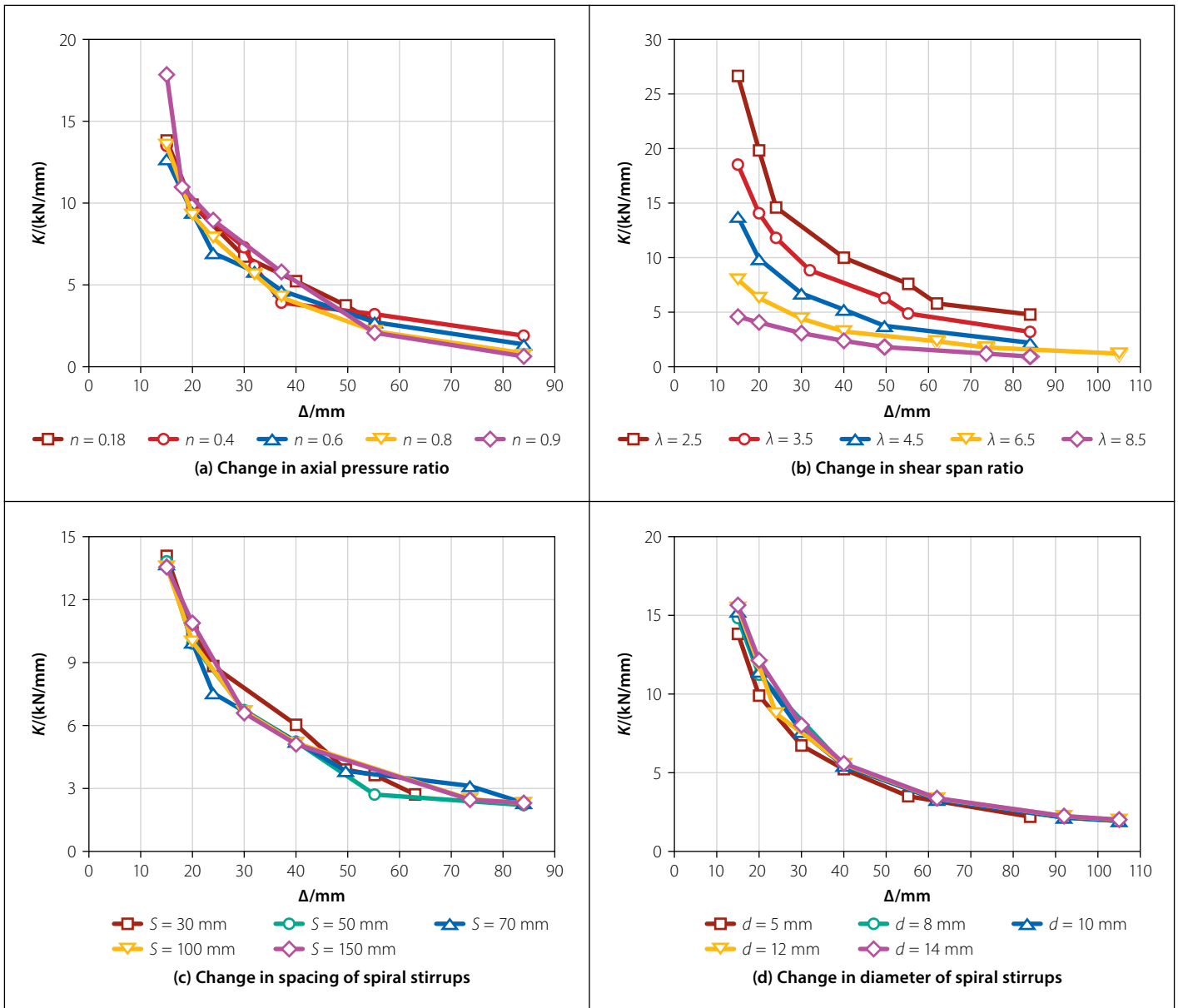2. As the λ increases, the failure of the specimen changes from shear failure

Figure 12 Stiffness degradation curve

to bending failure. Therefore, when the λ is small, the shear stiffness is greater, while the secant stiffness decreases at the same horizontal displacement.

3. The stiffness curves of the spacing and diameter of different rectangular spiral stirrups are basically similar, and the initial stiffness is almost coincidental, indicating that the contribution of rectangular spiral stirrups to the stiffness of the specimen is not significant at this time. This is consistent with the conclusion in existing literature that the influence of circular spiral stirrups on the stiffness of concrete columns is not significant (Xu 2021).

RESEARCH ON SIZE EFFECT

In order to make the numerical analysis more reliable, the seismic performance of specimens with larger and smaller

cross-sections was calculated. Figure 13 shows the comparison of hysteresis curves and concrete tensile damage for three different cross-sections. As shown in Figure 13(a), the plastic hinge zone of the small cross-section specimen is higher, which is due to the larger shear span ratio and the occurrence of compression bending failure. The collapse zone of the large cross-section specimen is higher because the shear span ratio is small and compression shear failure occurs. The above conclusion can also be seen in Figure 13(b) where the hysteresis curve of the small cross-section specimen is flatter, while the hysteresis curve of the large cross-section specimen is fuller.

LIMIT VALUE OF AXIAL COMPRESSION RATIO

Through the above parameter research, it can be seen that under different axial

compression ratios and shear span ratios, the deformation capacity of rectangular high-strength spiral reinforced concrete columns will be greatly affected. To ensure the deformation capacity of the columns, it is necessary to propose a matching relationship between the two. This paper is based on the standard that the ductility of reinforced concrete structures should not be less than 3.00 (Chinese Standard 2010b), and, through the trial calculation of nearly 100 specimens, the matching relationship between the final test axial compression ratio, design axial compression ratio, and shear span ratio is shown in Figure 14. Considering the load combination coefficient and material strength partial coefficient of 1.625, the design axial compression ratio limit value can be calculated. As shown in Figure 14, the critical axial compression ratio of the composite column gradually decreases as the shear span ratio increases. This can be attributed to the fact
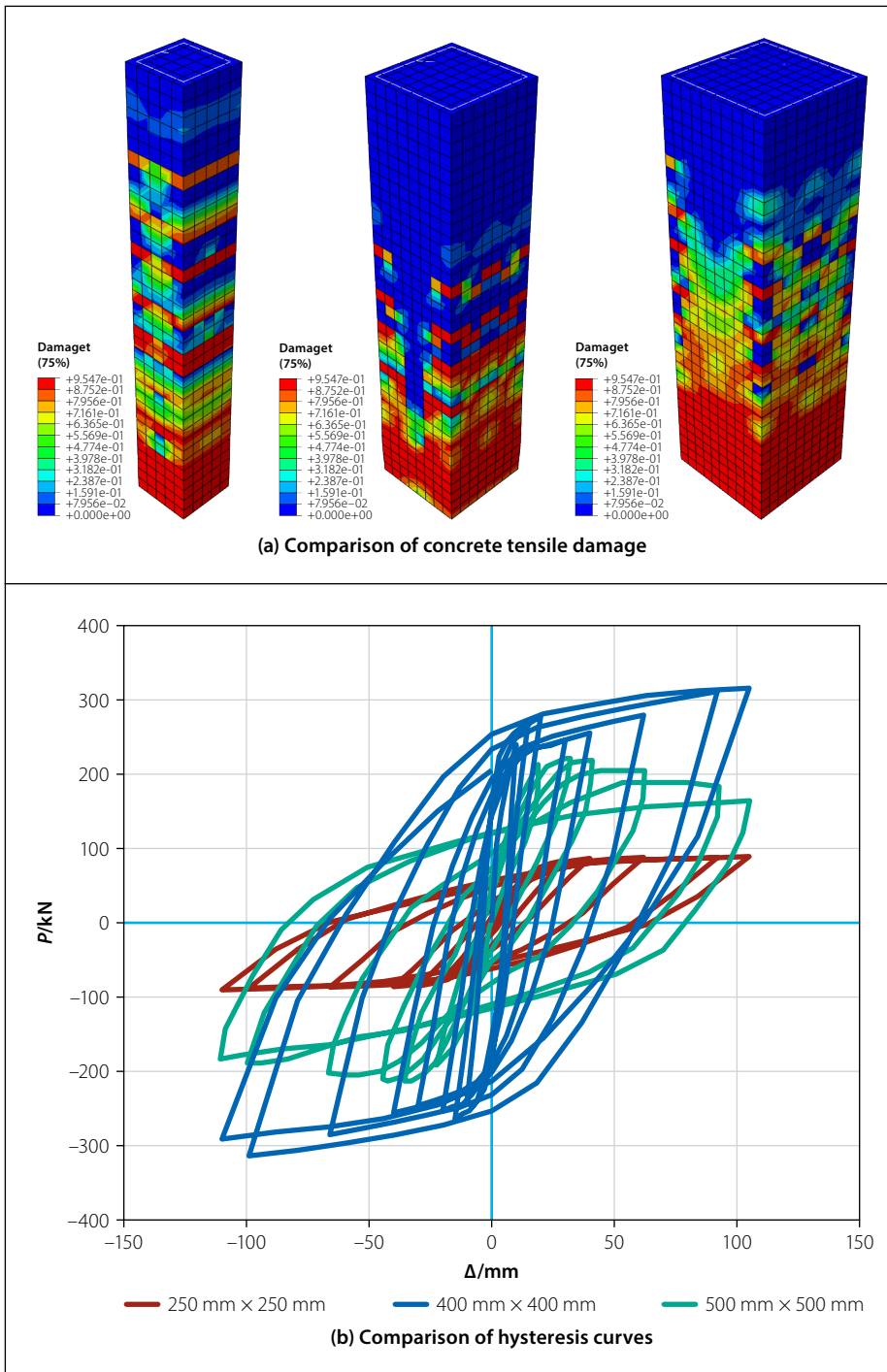
(a) Comparison of concrete tensile damage

(b) Comparison of hysteresis curves

Figure 13 Analysis results of size effect

that a larger shear span makes the column more slender, increasing its susceptibility to buckling. Therefore, an increase in the shear span ratio leads to a decrease in column stability. It is important to note that the degradation of the critical axial compression ratio is faster when the shear span ratio is between 2.5 and 4.5. This could be due to a change in the buckling mode of the column within this range. Specifically, the column may transition from a non-buckling state to a single- or hyperbolic-buckling state. Such a change in buckling mode results in a rapid decline in the bearing capacity of the column, and consequently a rapid decrease in the limit value of the axial compression ratio.

CONCLUSIONS

In this paper, the seismic performance FE analysis of 17 rectangular high-strength spiral reinforced concrete columns and the ductility analysis of nearly 300 specimens with different axial compression ratios and shear span ratios were completed, and the following conclusions are drawn:

1. Two specimens from previous literature were simulated and validated, and the reliability of the model was verified from failure modes, hysteresis curves, and skeleton curves. The stress analysis of the test specimen found that the longitudinal reinforcement stress curve is symmetric about the coordinate axis, while the

stress-strain curve of rectangular high-strength spiral stirrups yields on the compressive side. This indicates that, during the entire stress process, the high-strength rectangular spiral stirrup mainly increases the confinement on the compression side, while the tensile stress on the tension side is provided by the longitudinal reinforcement. The higher the axial compression ratio, the earlier the yield of the longitudinal reinforcement and spiral stirrup.

2. The bearing capacity and ductility of the specimen exhibit significant degradation due to the increase in axial pressure. When the axial compression ratio is not greater than 0.4, the ductility requirement of greater than 3 can be met. As the shear span ratio increases, the bearing capacity of the specimen gradually decreases, and the ductility is best when the shear span ratio is around 4.5. The changes in spacing and diameter of rectangular high-strength spiral stirrups have little impact on bearing capacity, but have a significant impact on ductility. It is recommended to have a stirrup ratio between 1.0% and 2.2%.

3. The initial shear stiffness increases with the increase of axial compression ratio, but the degradation rate is faster after reaching the peak. The greater the shear span ratio, the smaller the secant stiffness of the specimen at the same horizontal displacement. The changes in spacing and diameter of rectangular high-strength spiral stirrups have little effect on the specimen.

4. The simulation of about 100 specimens was completed to meet the criterion of ductility coefficient not less than 3. The matching relationship between the experimental axial compression ratio and the design axial compression ratio and the shear span ratio was proposed.

5. Due to the limited functionality of finite element software, it is not possible to consider more comprehensive and practical engineering situations. Therefore, it is recommended that the dynamic response or mechanical performance response of this type of composite column in frame structures should be studied further in future research.

AUTHOR CONTRIBUTION STATEMENT

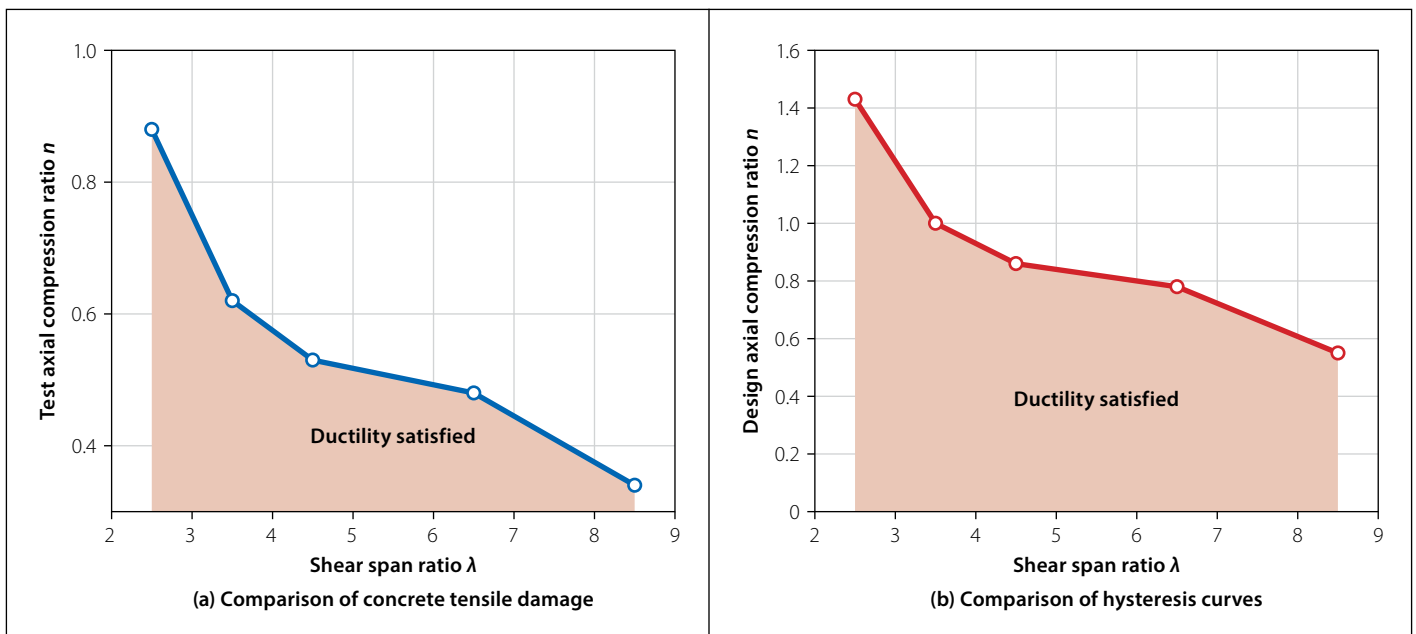Mengze Han: Conceptualisation, funding acquisition, writing original draft

Figure 14 Matching relationship between *n* and *λ*

Zicong Ma: Conceptualisation, formal analysis

Qirong Qiu: Data curation, formal analysis, writing review and editing

Pengcheng Liao: Software, data curation

CONFLICTS OF INTEREST

The authors have no conflicts of interest.

REFERENCES

Aboukifa, M & Moustafa, M A 2021. Experimental seismic behavior of ultra-high performance concrete columns with high strength steel reinforcement. *Engineering Structures*, 232: 111885. DOI: **10.1016/j.engstruct.2021.111885**.

Cao, Q, Li, X & Gao, R 2019. Axial compressive performance of CFRP confined self-stressing high-strength concrete cylinders. *KSCE Journal of Civil Engineering*, 23: 4000–4009. DOI: **10.1007/s12205-019-0039-9**.

Chen, Z, Zhou, J, Jing, C & Tan, Q 2021a. Mechanical behavior of spiral stirrup reinforced concrete filled square steel tubular columns under compression. *Engineering Structures*, 226: 111377.

Chen, Z, Xu, R, Ning, F & Liang, Y 2021b. Compression behaviour and bearing capacity calculation of concrete filled double skin square steel columns. *Journal of Building Engineering*, 42: 103022. DOI: **10.1016/j.jobe.2021.103022**.

Chen, Z, Chen, J, Xu, R & Li, Z 2022a. Mechanical behavior of square composite columns with four interlocking spirals under compression. *Journal of Building Engineering*, 46: 103740.

Chen, Z, Chen, J & Zhou, S 2022b. Experimental and numerical investigations on the behavior of a novel multilayer spirals reinforced square composite column under axial load. *Structures*, 43: 299–315.

Chen, Z, Chen, J, Xue, J & Mo, L 2022c. Experimental research and finite element analysis on seismic behavior of square reinforced concrete columns with four interlocking spirals. *Structures*, 39: 1–16.

Chen, Z, Xu, R & Liang, H 2022d. Residual mechanical properties and numerical analysis of recycled pebble aggregate concrete after high temperature exposure and cooled by fire hydrant. *Construction and Building Materials*, 319: 126137. DOI: **10.1016/j.conbuildmat.2021.126137**.

Chen, Z, Ke, X & Chen, Y 2015. Experimental study on seismic performance of steel reinforced high-strength concrete columns with rectangular spiral stirrups. *Journal of Civil Engineering*, 48(7): 41–49 and 59 (in Chinese).

Chinese Standard 2010a. *GB 50010-2010 Code for Design of Reinforced Concrete Structures.* Beijing: China Planning Press (in Chinese).

Chinese Standard 2010b. *GB 50011-2010 Code for Seismic Design of Buildings.* Beijing: China Construction Industry Press (in Chinese).

Guo, Z, Liu, Z & Che, X 2001. Experimental study on seismic behavior of reinforced concrete unit frames with square spiral stirrups under low cycle cyclic horizontal loading. *Journal of Building Structures*, 1: 8–13 and 25 (in Chinese).

Jing, L, Yin, S & Lv, H 2020. Bonding behavior of textile reinforced concrete (TRC): confined concrete and reinforcement under chloride erosion environment. *KSCE Journal of Civil Engineering*, 24: 826–834. DOI: **10.1007/s12205-020-0711-0**.

Mander, J B, Priestley, M J & Park, R 1988. Theoretical stress-strain model for confined concrete. *Journal of Structural Engineering*, 114(8): 1804–1826.

Su, J, Wang, J & Wang, W 2014. Experimental study on seismic performance of concrete columns restrained by high-strength spiral stirrups. *Earthquake Engineering and Engineering Vibration*, 34(4): 206–211 (in Chinese).

Xu, R 2021. Study on mechanical properties of self-compacting concrete with CFRP-PVC spiral reinforcement composite restraint. Report. Nanning, China: Guangxi University.

Xue, J, Li, H, Ke, X & Chen, Z 2016. Pseudostatic test and finite element analysis of high-strength steel concrete columns with rectangular spiral stirrups. *Industrial Architecture*, 46(2): 133–138 and 175.

Xue, J, Zhang, X & Ke, X 2019. Seismic resistance capacity of steel reinforced high-strength concrete columns with rectangular spiral stirrups. *Construction and Building Materials*, 229: 116880. DOI: **10.1016/j.conbuildmat.2019.116880**.

Xue, J, Zhao, X & Ke, X 2020. Experimental and numerical investigation of high-strength concrete encased steel columns with rectangular-spiral stirrups. *Journal of Building Engineering*, 32: 101518. DOI: **10.1016/j.jobe.2020.101518**.

Yang, C, Chou, Y C & Hung, C C 2022. Seismic behavior of full-scale wall piers with high-strength steel reinforcement. *Engineering Structures*, 256: 114068. DOI: **10.1016/j.engstruct.2022.114068**.

Zhang, X, Zheng, X & Pan, S 2013. Seismic performance test of high-strength spiral stirrup confined concrete columns. *Journal of Building Science and Engineering*, 30(2): 21–27 (in Chinese).

Zhao, H, Li, Q, Weishan, J & Xinghu, Z 2019. Research on seismic performance of high-strength concrete shear walls with high-strength spiral reinforcement constraints. *Journal of Building Structures*, 39(4): 54–64 (in Chinese).